

Towards a precise measurement of the antihydrogen ground state hyperfine splitting in a beam: the case of in-flight radiative decays

R Lundmark¹, C Malbrunot^{2,3}, Y Nagata⁴, B Radics⁴, C Sauerzopf³ and E Widmann³

¹ Department of Fundamental Physics, Chalmers University of Technology, 412 96 Göteborg, Sweden

² CERN, Genve 1211, Switzerland

³ Stefan-Meyer-Institut für Subatomare Physik, Österreichische Akademie der Wissenschaften, Wien 1090, Austria

⁴ Atomic Physics Laboratory, RIKEN, Saitama 351-0198, Japan

E-mail: rikard@rikardlundmark.com and chloe.m@cern.ch

Received 23 February 2015, revised 7 May 2015

Accepted for publication 29 May 2015

Published 29 July 2015



CrossMark

Abstract

The ASACUSA antihydrogen setup at the CERN Antiproton Decelerator (AD) consists of an antihydrogen source (cusp magnet coupled to a positron source and an antiproton catching magnet) followed by a spectrometer beamline. After production in the cusp, the antihydrogen atoms decay while they escape the trap leading to changes in their effective magnetic moment which in turn affect their trajectories in the beamline. Those sequential decays in the presence of a varying magnetic field strength from their production point in the cusp to their detection at the end of the spectrometer line can in principle greatly affect the prospects for a precision measurement of the antihydrogen hyperfine splitting given the so-far relatively low number of available anti-atoms. The impact of the antihydrogen decay in this context has for the first time been simulated. The implementation of atomic radiative decay has been done in *Geant4* to extend the particle tracking capabilities originally embedded in *Geant4* to excited atoms, and to allow studies of the effect of dynamic atomic properties on trajectories. This new tool thus allows the study of particle–matter interaction via the *Geant4* toolkit while properly taking into account the atomic nature of the object under study. The implementation as well as impacts on the experimental sensitivity for antihydrogen spectroscopy are discussed in this paper.

Keywords: antihydrogen, radiative decay, ground state hyperfine splitting measurement

1. Introduction

The ASACUSA collaboration aims at measuring the ground state hyperfine splitting of antihydrogen using a Rabi-like experimental setup [1, 2] at CERN as a test of CPT symmetry. According to the CPT theorem, hydrogen and antihydrogen

should have the same energy spectrum. Therefore any observed difference would be an indication of CPT violation. Some extensions of the standard model allow for such symmetry breaking [3, 4].

Recently the ASACUSA-cusp collaboration reported the detection of 80 antihydrogen atoms 2.7 m away from the production point [5] which is a milestone towards the formation of an intense beam and the start of the spectroscopy measurement campaign. So far however the accumulated number of antihydrogen atoms at the detector is very low and their velocity and quantum distribution at production is



Content from this work may be used under the terms of the Creative Commons Attribution 3.0 licence. Any further distribution of this work must maintain attribution to the author(s) and the title of the work, journal citation and DOI.

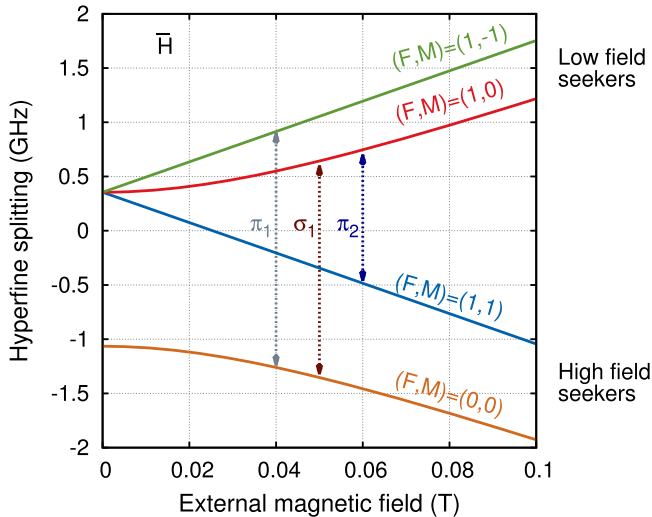


Figure 1. Ground state hyperfine splitting in antihydrogen.

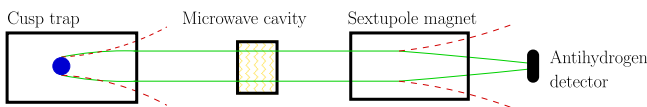


Figure 2. Schematic view of the experimental setup (color online). Antihydrogen is formed in an antiproton–positron plasma inside the cusp trap (blue circle). HFS antihydrogen will follow the red dashed trajectories and eventually annihilate on the beampipe. LFS antihydrogen will follow the green solid lines through the microwave cavity and the sextupole magnet, and hit the antihydrogen detector at the end of the beamline. If the microwave cavity is tuned to the very frequency of transition from HFS to LFS (see figure 1), the antihydrogen will be converted to HFS and the sextupole magnet will bend it resulting in a loss of signal at the antihydrogen detector. For the simulation results presented in this paper, the microwave cavity is always turned off.

unknown. In this context, a reliable simulation of the antihydrogen atoms from their production point to their detection is necessary. The addition of atomic radiative decay to the already existing *Geant4* simulation of the ASACUSA-cusp apparatus enables realistic simulations on the quantum state of the atom during its flight toward the detector and enables the extraction of information on the polarization and velocity of the antihydrogen beam at the detector.

The ground state energy levels of antihydrogen vary in a magnetic field as depicted in figure 1. Depending on the coupling between the antiproton and positron spins, the energy will decrease or increase with the magnetic field. We denote the states that have decreasing energies with increasing magnetic field as ‘high-field seeker’ (HFS) states and the states with increasing energies as ‘low-field seeker’ (LFS) states. The splitting of antihydrogen hyperfine states in the presence of a magnetic field is a key feature used to characterize and precisely measure the physical properties of antihydrogen.

The ASACUSA-cusp experimental setup is shown in figure 2. Antihydrogen is formed in a so-called cusp trap [6] where a magnetic field and an electric potential confine a positron–antiproton plasma. The magnetic field gradient in

the cusp trap will predominantly focus LFS antihydrogen atoms towards the microwave cavity, while HFS atoms will be bent away [7]. In the microwave cavity, antihydrogen may flip from LFS to HFS if the radiofrequency matches the energy difference between the energy levels. The sextupole magnet will then focus LFS antihydrogen atoms to the detector, and bend away HFS ones. By scanning the radiofrequency, one would be able to note a dip in the the number of detected antihydrogen atoms at the detector when the frequency matches the energy level splitting of antihydrogen, and thereby the level splitting can be determined [8].

This Rabi-like experiment has the advantage of being suitable for antihydrogen with relatively high temperatures (up to ~ 100 K), unlike experiments working with trapped atoms (e.g. ALPHA [9, 10], ATRAP [11]) which require very cold antihydrogen (≤ 0.5 K).

A detailed geometry of the apparatus is implemented in *Geant4* [12] as shown in figure 3 [13]. Particles are transported by numerically solving their associated equations of motion in discrete steps, and Monte Carlo methods are used for the physical processes involved. *Geant4* does not allow for changes in the inherent properties of a particle. This is a crucial feature needed to model excited atoms, and atoms that undergo radiative deexcitation, such as the antihydrogen produced in the cusp trap. Without knowledge of the quantum state of the particle in question, the trajectory and beam polarization cannot be determined accurately. In this paper, we describe the implementation of excited quantum states of atomic antihydrogen in the existing *Geant4* simulation. The impact on the beam polarization as well as the signal and background at the antihydrogen detector have been evaluated for different initial experimental parameters. We show that the implementation indeed gives significantly different results when compared to cases in which the de-excitation was neglected.

2. Theory

In a magnetic field, the antihydrogen Hamiltonian H can be expanded perturbatively as $H = H_0 + V_M$ where H_0 is the unperturbed Hamiltonian and $V_M = -\mathbf{B} \cdot \boldsymbol{\mu}$ with \mathbf{B} as the magnetic field and $\boldsymbol{\mu}$ as the magnetic moment of the atom. With a position-dependent magnetic field $\mathbf{B} = \mathbf{B}(\mathbf{r})$ and magnetic moment $\boldsymbol{\mu} = \boldsymbol{\mu}(\mathbf{r})$, the force on the atom can be expressed as $\mathbf{F} = \nabla(\boldsymbol{\mu} \cdot \mathbf{B})$.

The term V_M can in theory be calculated for antihydrogen in a magnetic field using numerical methods. However, we have chosen another approach and assigned a set of quantum numbers to antihydrogen atoms in order to derive their magnetic moments and decay lifetimes to the ground state. The good set of quantum numbers depends of course on the external magnetic field strength.

2.1. Weak magnetic field

In the weak field limit, the spin–orbit interaction dominates and the weak-field Zeeman effect can be used to a good

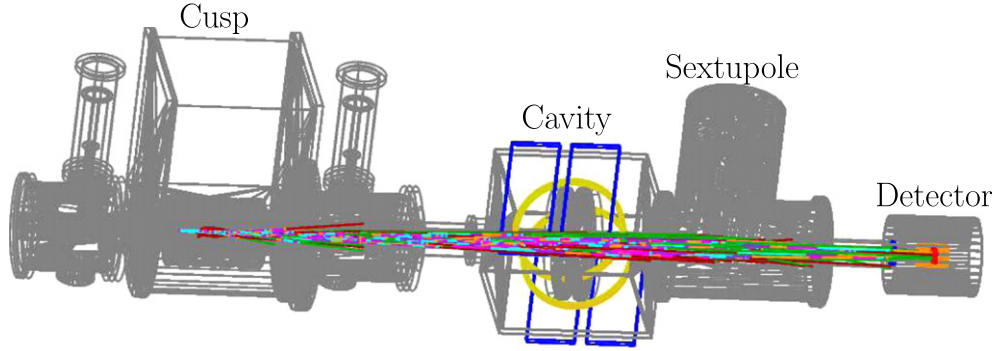


Figure 3. Simulated antihydrogen atom trajectories through the ASACUSA-cusp apparatus (color online). The colored (gray) tracks represent antihydrogen atoms, and a change in color (tone) represent a change in the principal quantum number n . The experimental setup can be compared to figure 2. Green and red tracks correspond to ground state LFS and HFS antihydrogen, respectively. Other colors indicate higher excited states.

approximation. A state is written as $|n, l, j, m_j\rangle$ where n is the principal quantum number, l is the orbital angular momentum quantum number, j is the total angular momentum quantum number and m_j is the secondary total angular momentum quantum number ranging from $-j$ to $+j$.

In an excited state $|n, l, j, m_j\rangle$ the projection of $\boldsymbol{\mu}$ on the magnetic field is calculated as $\mu_z = m_j g_j \mu_B$ where

$$g_j = g_l \frac{j(j+1) - s(s+1) + l(l+1)}{2j(j+1)} + g_s \frac{j(j+1) + s(s+1) - l(l+1)}{2j(j+1)}$$

using $g_l = 1$, $g_s \approx 2$ and $s = \pm \frac{1}{2}$.

Here, we approximated the contribution from the nuclear magnetic moment to zero. This is reasonable, since it is of the order of the electron mass divided by the proton mass smaller than the Bohr magneton.

2.2. Strong magnetic field

In the strong field (Paschen–Back) limit, the effects of the magnetic field dominate over the spin–orbit interaction. A proper state now uses the quantum numbers $|n, l, m_l, m_s\rangle$ where n and l are as above, and m_l and m_s are the eigenvalues of the angular momentum and spin operators, respectively. The magnetic moment projection on the magnetic field is now calculated as $\mu_z = (g_l m_l + g_s m_s) \mu_B$ [14, p 330].

2.3. Intermediate magnetic field

If neither of the terms dominate, we assumed both sets of quantum numbers to be valid. This assumption has been validated by changing the size and location of the intermediate region in the simulation and observing a small effect on the result. In order to determine when the Zeeman term or spin–orbit term dominate, and thereby determine which set of quantum numbers to use when labeling a state, a comparison is done between the strong or weak energy splitting in the magnetic field and the fine structure splitting term of

antihydrogen. This latter is given by

$$\Delta E = -13.6 \text{ eV} \frac{\alpha^2}{n^2} \left(\frac{1}{j + \frac{1}{2}} - \frac{3}{4n} \right)$$

where α is the fine structure constant.

3. Calculating the deexcitation rates

The deexcitation rates of antihydrogen in a magnetic field depend on the field strength. The rates are calculated using a modified version [15] of a software package called Flexible Atomic Code (FAC) written in C [16].

We modified the FAC software further so that selected parts of it compiled as C++-code. It was also modified to accept orbital quantum numbers higher than $l = 22$, which was the initial limit. The code was used to generate transition rate tables for various magnetic field strengths. The FAC output was in the form of a large number of binary files. These were transferred to a ROOT [17] tree, which was then used to create optimized interpolation objects. These objects were saved in another ROOT tree, which could be loaded directly into the simulation of the ASACUSA experimental setup. The deexcitation rates were calculated for all allowed dipole transitions. Filtering out very improbable transitions (with an Einstein A coefficient less than 10^{-3} s^{-1}) reduced the database size by about one order of magnitude. The final result was a ~ 100 MB ROOT file which could be loaded into the Geant4 simulations. A cross-check of the deexcitation rate calculation was performed for zero field strength using a random sample of data from the NIST atomic database [18]. The mean relative error was negligible (approximately 10^{-3}).

The lifetime of the excited states ranges from the order of nanoseconds for some small values of n , to the order of milliseconds for n close to 30 and circular states (with maximum orbital and magnetic quantum numbers). For the ASACUSA application, we have generated a database of decay rates at different magnetic fields in the range of interest up to principal quantum number $n = 42$. In practice, as will

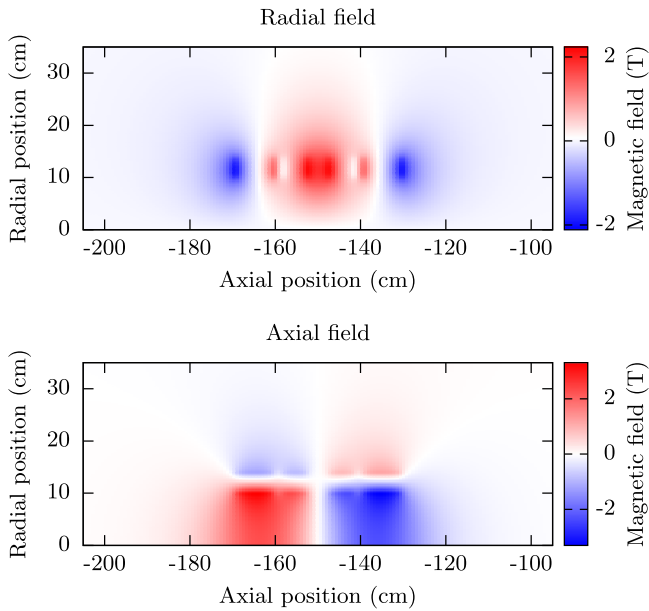


Figure 4. Magnetic fields inside the cusp trap. Positions are relative to the center of the cavity. Antihydrogen is produced at $z = -165$ cm and the beam travels toward positive z .

become clear later in this paper, the region of interest down to very small kinetic energies (antihydrogen temperature of the order of 10 K) lies below principal quantum number $n = 30$.

4. Simulation

In *Geant4* a particle is usually represented as a static singleton object which is not supposed to be modified. In order to circumvent this restriction we assign changeable quantum numbers to the particle. Using the database calculated with FAC, antihydrogen atoms are allowed to cascade down to lower quantum states from an arbitrary initial state. This cascading can be made to depend on the external magnetic field by having the object representing the particle itself keep track of the magnetic field at each step in the simulation. After each deexcitation, the time until the next deexcitation as well as the next decay channel is calculated right away. This is done probabilistically by using the magnetic field at the particle's current position in conjunction with the deexcitation database. At each discrete step along the particle's trajectory, the particle object is reminded of the elapsed time since the last step, and can cascade to lower states. This cascading can happen several times within a single step and will take place until the accumulated time for all deexcitations exceeds the total accumulated time since the particle was created.

The standard *Geant4* equation of motion is modified to take the force on a neutral atom into account. An excited state in antihydrogen can have a radically different magnetic moment than an antihydrogen atom in the ground state. The magnetic force exerted on the atom will therefore depend on its quantum state, as discussed above. Figure 4 shows the radial and axial component of the magnetic field inside the cusp trap, where antihydrogen is produced. The small change

in momentum of an antihydrogen atom due to the recoil upon transition is ignored, since it is orders of magnitude smaller than the momentum corresponding to the most probable speed for an antihydrogen atom with a temperature between 10 and 100 K.

For each time step in the simulation additional tracking information about the antihydrogen state had to be stored separately for analysis and track reconstruction since this information would otherwise be lost once the singleton particle has changed its state. Figure 3 illustrates the changes in the antihydrogen principal quantum number along the trajectory of the atom.

In the simulation, translation from weak field quantum numbers to strong field quantum numbers is made when the Zeeman term exceeds the hyperfine splitting term by a constant factor. Translation in the other direction is done in the same way, but with another constant factor, creating a hysteresis region to prevent multiple translations during a short period of time. The translation is done according to the appropriate Clebsch–Gordan coefficients which indicate the transition probabilities for each state.

We should point out that so-called Majorana spin flips (a spontaneous deexcitation provoked when the atom magnetic moment does not adiabatically follow the field direction) have been neglected in the simulation since their contributions should be very small at antihydrogen temperatures below 100 K [7].

The step size for which the equation of motion is solved to calculate the antihydrogen trajectories in the simulation was 5 mm, except in the cusp where it was reduced to 10 μm to accommodate for the large magnetic field gradients. The magnetic field inside the cusp trap was discretized with a radial mesh size of 0.5 mm and an axial mesh size of 1.5 mm. A linear interpolation was done between the discrete points.

5. Results & discussions

The distribution of the antihydrogen quantum states directly after its formation from positrons and antiprotons in the cusp trap is not fully known. From previous measurements [5] and antihydrogen formation simulations ([19–21] and references therein), it is known that at least a portion of the antihydrogen atoms are formed in Rydberg states. In order to evaluate the effect of producing excited antihydrogen on the measured signal at the detector, we have assumed different initial quantum states and compared the results. Since the temperature of the produced antihydrogen atoms is not known either, we also evaluated the performance at different initial velocities. In this paper we present results for a mono-velocity beam. In the simulation, for each velocity, the magnetic field of the sextupole magnet is adjusted to focus the ground state low field-seeking antihydrogen atoms onto the detector. For an initial velocity corresponding to the most probable velocity of a Maxwell–Boltzmann distribution for temperature of $\theta = 10$ K and $\theta = 50$ K, the sextupole field peak value is adjusted to 0.35 T and 1.675 T, respectively. Some key parameters used in the simulations can be found in table 1.

Table 1. Parameters used in the simulation. Distances are given along the symmetry axis z and relative to the center of the microwave cavity. Particles travel in a direction of increasing z .

Parameter	Value
Sextupole magnet inner diameter	10 cm
Antihydrogen production point	−165 cm
Detector position	150 cm
Beam opening angle ^a	2°

^a Maximum possible angle between the initial antihydrogen velocity vector and a vector pointing from the cusp trap to the detector along the symmetry axis. Each allowed direction for the velocity vector is equally probable.

The performance of the setup can be characterized by the fraction of the antihydrogen atoms initially in the cusp reaching the detector after passing the cavity in ground state (signal) and the percentage reaching the detector after passing the cavity in an excited state (background). Figures 5 and 6 show respectively the signal and the background at the detector as a function of the initial principal quantum numbers at the production point. Figure 5 includes two initial velocities for comparison.

For small initial principal quantum numbers, the lifetimes of each state are very short. Therefore, the atoms thus produced will decay to ground state almost instantaneously after production and will generate very similar signals in the detector to the ones of atoms produced in ground state in the cusp. This is the reason for the flatness of the curves in figure 5 for low values of n . Furthermore, strong HFS/LFS states (labeled as sLFS/sHFS, see the caption of figure 5 for definition) have a low probability of spin flip (changing from LFS to HFS or vice versa) for each decay step while weak HFS/LFS have a probability of the order of $\frac{1}{2}$. This explains why the signal at the detector is about 50% of the initial number of atoms for weak HFS/LFS. As mentioned earlier, the apparatus is designed to select away high field-seeking states. Consequently all strong LFS states produced with relatively low n (with the parameters listed in table 1) will reach the detector (given the beam opening angle chosen for this study, see table 1) while almost none of the strong HFS will reach it as shown in figure 5.

With larger initial principal quantum numbers, atoms travel further down the experimental setup before reaching ground state. Atoms reaching HFS ground state will be selected away by the sextupole while those reaching LFS ground state will hit the detector and contribute to the signal or background. Those observables will therefore be affected by the longer time the atoms with a large magnetic moment (i.e. antihydrogen atoms in an excited state) spend in the cusp. In the cusp magnetic field the low field seeker atoms with large magnetic moments will indeed be accelerated as shown in the bottom plot of figure 7. The atoms will thus exit the cusp with a larger mean velocity and subsequently enter the sextupole magnet with a broader velocity spread. In this case, a larger number of atoms will be bent away from the detector as shown in the top plot of figure 7. This in part explains the

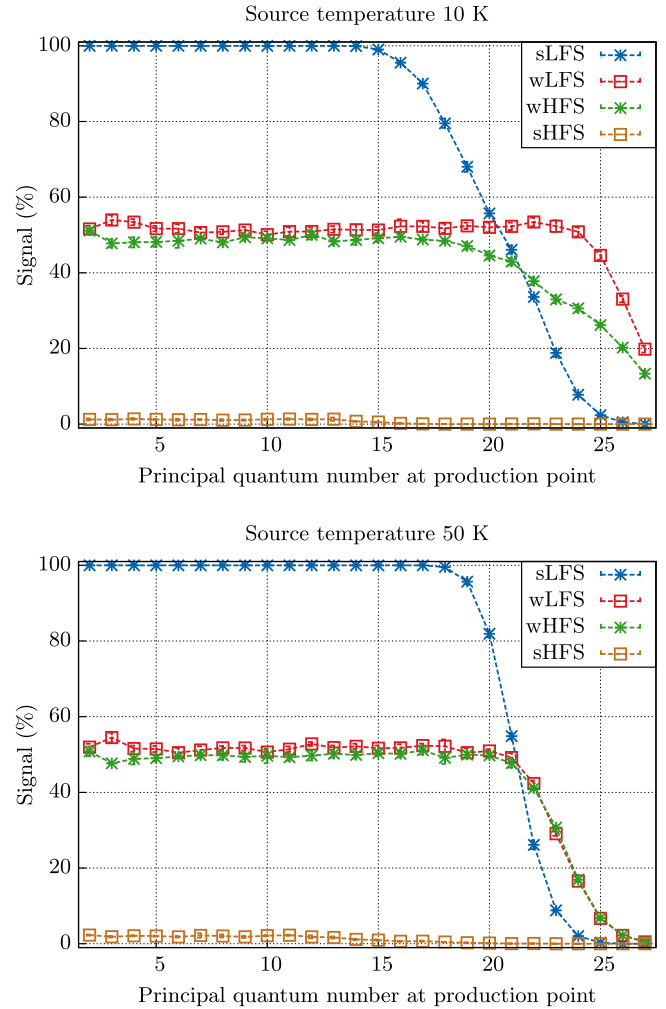


Figure 5. Percentage of produced atoms reaching the detector after passing the cavity in ground state (signal). The principal quantum number at the production point is indicated on the x -axis, and the orbital quantum number is initially always set to $l = n - 1$. Results for four different choices of quantum numbers are shown. They are labeled according to how strongly they react to an applied magnetic field: w = weak (magnetic quantum number $m_j = \pm \frac{1}{2}$) and s = strong ($m_j = \pm j$). The initial velocity corresponds to the most probable velocity for the temperature indicated. Statistical error bars are included.

steep drop for the sLFS curves in figure 5. For weak LFS or HFS atoms, these accelerating/decelerating effects will be weaker, which explains why the drop in these curves is not as steep, even though wLFS/HFS states tends to decay faster than sLFS/HFS. The reason for the later and steeper drop in the 50 K curves compared to the 10 K curves is the following: faster antihydrogen atoms will exit the cusp magnetic field before the slow ones. These atoms will therefore have less time than the colder atoms to decay in the cusp magnetic field. The smaller number of possible occupied quantum states will in turn produce antihydrogen atoms at the exit of the cusp with a smaller velocity spread and will lead to a stronger signal at the detector. This mechanism reaches a limit when the antihydrogen atoms do not have enough time on average to decay to ground state before they reach the cavity. In that

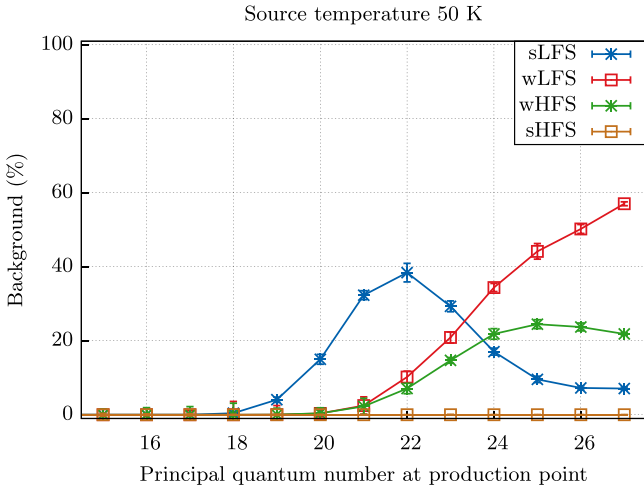


Figure 6. Percentage of produced atoms reaching the detector after passing the cavity in an excited state, which will effectively be a source of background at the detector. The notation is the same as in figure 5.

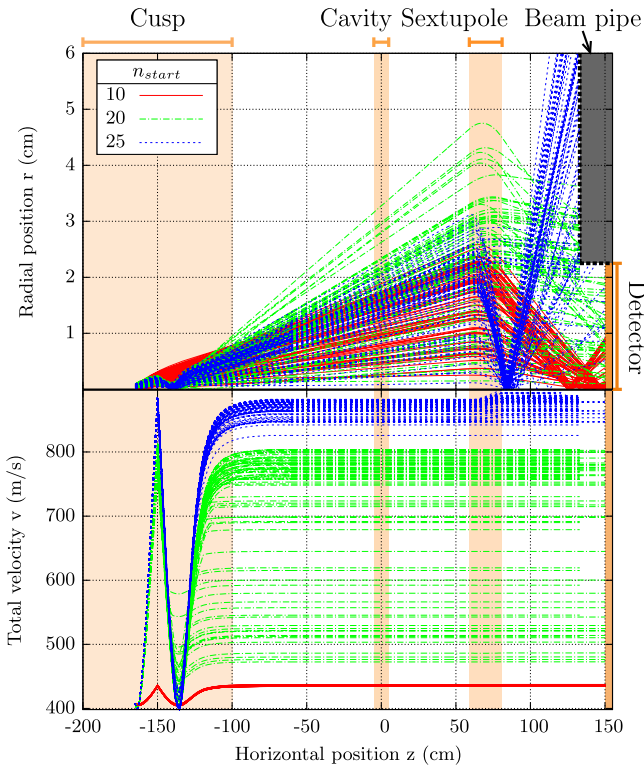


Figure 7. Radial coordinate (top) and total velocity (bottom) as a function of the axial coordinate z for three different initial quantum numbers n for sLFS atoms using a source temperature of 10 K. Note the beam pipe at $z = 133$ cm in the top figure which blocks atoms diverging too much from the axis from reaching the detector. The effect of the beam pipe is also visible in the lower figure, where many tracks stop before reaching the detector.

case the loss of signal is faster as a function of the n state for a 50 K than for a 10 K beam.

Finally, for even larger n the atoms will be less likely to reach ground state before passing the microwave cavity, and

will therefore not be counted as signals in the simulation, but as background. Figure 6 illustrates this behavior at 50 K. One can observe that at this velocity the background for sLFS peaks at $n = 22$. This is the limit at which the atoms can reach the sextupole in ground state even though they passed the cavity in an excited state. Since the sextupole is tuned to focus ground state LFS, atoms with a larger magnetic moment will be over-focused and therefore less likely to reach the detector which leads to a reduced background. This is a remarkable result which indicates that there exist particularly unfavorable sets of initial quantum numbers.

The signal and background at the detector are useful observables which can be corroborated with experimental data. However, we want to emphasize that the quantitative results presented here are dependent on the choice of simulation parameters. In particular, results were presented for a mono-energetic beam of antihydrogen atoms to somewhat simplify the interpretation. A more realistic velocity distribution may lead to a reduction in the signal which will be dependent on the velocity and initial quantum number distributions. For example, the signal for sLFS atoms produced in an $n = 20$ state with a Maxwell-Boltzmann distributed velocity for a temperature of 50 K would be $\sim 66\%$ compared to $\sim 80\%$ for a mono-velocity beam as shown in the bottom panel of figure 5 (all other simulation parameters alike).

An important parameter for the ASACUSA experiment which can also be extracted via this simulation is the averaged polarization of the antihydrogen beam at the exit of the cusp. Previous studies which did not take into account excited antihydrogen states and their decays in the cusp suggest that the polarization degree of the antihydrogen atoms at the entrance of the cavity is $\mathcal{P} = \frac{f_{\text{LFS}} - f_{\text{HFS}}}{f_{\text{LFS}} + f_{\text{HFS}}} \sim 30\%$ for an antihydrogen temperature of 50 K (assuming an equal number of produced ground state LFS and HFS) [7, 22] where f_{LFS} and f_{HFS} are respectively the fraction of LFS and HFS states recorded. We have simulated antihydrogen atoms with initial sLFS and sHFS states and with two different initial principal quantum numbers: $n = 15$ and $n = 20$ (using the simulation parameters listed in table 1). We found that the polarization \mathcal{P} for ground state antihydrogen at the entrance of the cavity was varying from $\sim 10\%$ (for $n = 15$) to $\sim 70\%$ (for $n = 20$). Those values are of course very dependent on the initial quantum state distribution chosen and the simulation parameters (beam opening angle, temperature, etc). This result however suggests that the production of excited antihydrogen states in the cusp has a sizeable impact on the polarization performances of the cusp. We have verified that the simulation of ground state antihydrogen atoms emitted isotropically leads to the same polarization at the entrance of the cavity as stated in [7].

The scope of this paper is restricted to the combined effect of magnetic fields and radiative decays on excited antihydrogen atoms' trajectories. The cusp trap also contains electric fields which may affect the deexcitation rates and trajectories of excited atoms. This effect could be incorporated in the simulation in a similar fashion as was described here for magnetic fields, taking into account the position-dependent angle between the electric and magnetic fields. A

study of this combined effect for particular field configurations and decay channels has been done for Rydberg antihydrogen atoms in traps [23].

6. Conclusion

In this paper, we have described the first implementation of excited antihydrogen states in a `Geant4` simulation. The implementation was used to investigate how the trajectories of antihydrogen atoms in the ASACUSA experimental setup would be affected by the change of their magnetic moment as they decay through the beamline. Changes in the antihydrogen trajectories in turn affect the polarization at the entrance of the cavity and the signal at the detector which are important parameters in the experiment that need to be thoroughly optimized given the scarcity of those anti-atoms. If the antihydrogen atoms are created with large principal quantum numbers ($n \gtrsim 20$ for $\Theta \lesssim 50$ K), the signal at the detector will be significantly reduced. We can conclude from this result that a method to produce antihydrogen in low excited states either within the cusp or at its exit should be implemented in order to increase the significance of the signal at the detector.

In order to predict the signal and background at the detector using the tool herein described, the initial distribution of the n , l and m quantum numbers and the velocity of produced antihydrogen atoms should be known either theoretically or experimentally. Investigating this, both theoretically and experimentally, is currently a strong focus of the ASACUSA collaboration.

Acknowledgments

The authors would like to thank E Stambulchik for providing a modified version of the `FAC` software and for valuable theoretical input. This work is supported by the European Research Council grant no. 291242-HBAR-HFS, the Austrian Federal Ministry of Science, Research and Economy, the

Grant-in-Aid for Specially Promoted Research (no. 24000008) of the Japan Society for the Promotion of Science (JSPS) and Pioneering Project of RIKEN.

References

- [1] Widmann E *et al* 2001 (*The Hydrogen Atom Lecture Notes in Physics* vol 570) ed S Karshenboim *et al* (Berlin: Springer) 528–42
- [2] Widmann E, Hayano R, Hori M and Yamazaki T 2004 *Nucl. Instrum. Methods Phys. Res. Sect. B* **214** 31
- [3] Colladay D and Kostelecky V A 1997 *Phys. Rev. D* **55** 6760
- [4] Bluhm R, Kostelecky A, Lane C and Russell N 2001 (arXiv: [hep-ph/0111141](https://arxiv.org/abs/hep-ph/0111141))
- [5] Kuroda N *et al* 2014 *Nat. Commun.* **5** 2
- [6] Mohri A and Yamazaki Y 2003 *Europhys. Lett.* **63** 207
- [7] Nagata Y and Yamazaki Y 2014 *New J. Phys.* **16** 083026
- [8] Widmann E *et al* 2013 *Hyperfine Interact* **215** 1
- [9] Andresen G B *et al* 2010 *Nature* **468** 673
- [10] Amole C *et al* 2012 *Nature* **483** 439
- [11] Gabrielse G *et al* ATRAP Collaboration 2012 *Phys. Rev. Lett.* **108** 113002
- [12] Agostinelli S *et al* 2003 *Nucl. Instrum. Methods Phys. Res. Sect. A* **506** 250
- [13] Malbrunot C *et al* 2014 *Hyperfine Interact* **228** 61
- [14] Sakurai J J 1994 *Modern Quantum Mechanics* (Reading, MA: Addison-Wesley)
- [15] Stambulchik E 2013 *Personal Communication with B Radics* Weizmann Institute of Science
- [16] Gu M F 2008 *Can. J. Phys.* **86** 675
- [17] Brun R and Rademakers F 1997 *Nucl. Instrum. Methods Phys. Res. Sect. A* **389** 81
- [18] Kramida A, Ralchenko Y and Reader J 2014 *NIST ASD Team, NIST Atomic Spectra Database (ver. 5.1)* (Gaithersburg, MD: National Institute of Standards and Technology) <http://physics.nist.gov/asd>
- [19] Robicheaux F 2008 *J. Phys. B: At. Mol. Opt. Phys.* **41** 192001
- [20] Robicheaux F 2008 *Phys. Rev. A* **70** 022510
- [21] Radics B, Murtagh D J, Yamazaki Y and Robicheaux F 2014 *Phys. Rev. A* **90** 032704
- [22] Enomoto Y *et al* 2010 *Phys. Rev. Lett.* **105** 243401
- [23] Henry M A and Robicheaux F 2011 *J. Phys. B: At. Mol. Opt. Phys.* **44** 145003